HHS Public Access

Author manuscript

Nanoscale. Author manuscript; available in PMC 2021 November 11.

Published in final edited form as:

Nanoscale. 2019 November 28; 11(46): 22172–22181. doi:10.1039/c9nr08510f.

Effective detection of bacteria using metal nanoclusters

Dan Li[a,b,#], **Beena Kumari**[a,c,#], **Jessa Marie Makabenta**[a], **Akash Gupta**[a], **Vincent Rotello**[a,*]

[a.]Department of Chemistry, University of Massachusetts Amherst,710 North Pleasant Street, Amherst, Massachusetts 01003, USA.

[b.]Department of Basic Science, Jinzhou Medal University, 40 Songpo Road, Jinzhou, China 121001, China.

[c.]Department of Chemistry, Indian Institute of Technology Gandhinagar, India

Abstract

Antibiotic-resistant bacterial infections cause more than 700,000 deaths each year worldwide. Detection of bacteria is critical in limiting infection-based damage. Nanomaterials provide promising sensing platforms owing to their ability to access new interaction modalities. Nanoclusters feature sizes smaller than traditional nanomaterials, providing great sensitive ability for detecting analytes. The distinct optical and catalytic properties of nanoclusters combined with their biocompatibility enables them as efficient biosensors. In this review, we summarize multiple strategies that utilize nanoclusters for detection of pathogenic bacteria.

1 Introduction

Bacterial infections cause more than a million illnesses and 20,000 deaths annually in the United States alone, costing $50–70 billion per year.[1, 2] The rapid increase of bacterial infections require facile and cost-effective detection strategies.[3–7] Current techniques to detect bacteria include polymerase chain reaction (PCR) and sequencing, which are costly and time-consuming.[8–12] Optical and electrochemical detection methods using organic dyes and traditional nanoparticles (NPs) provide facile strategies for analysis of bacteria. However, these sensors are often associated with toxicity and low sensitivity, limiting their practical applications.[13–19]

When NPs are composed of a small number of atoms, the as-obtained materials are denoted as nanoclusters (NCs) (Figure 1).[20] The size of NCs are normally < 2 nm. Significantly for both biomedical and environmental concerns, NCs show minimal organ retention and accumulation.[21–23] The physiochemical and optoelectronic properties of NCs are significantly different from their larger counterpart (NPs).[24–27] For instance, gold NCs (AuNCs) do not exhibit surface plasmon resonance (SPR) like traditional gold NPs (AuNPs).[28] On the other hand, AuNPs do not exhibit fluorescence, unlike many of their

* rotello@chem.umass.edu .

Both authors contribute equally to this work.

Conflicts of interest

There are no conflicts to declare.

smaller AuNC counterparts. These optical differences are caused by many factors such as the quantum confinement effect, discrete energy levels, ligand-to-metal and metal-to-metal charge transfer, the synergistic effect between the protection ligand and the metal core, and additional mechanisms that are still under investigation.[29–32] Another important property possessed by NCs is their enhanced catalytic activity compared to NPs.[33–39] The catalytic properties of metal catalysts are influenced by the size of particles. For instance, small size palladium NCs (PdNCs) are more active than the larger palladium NPs (PdNPs).[40] These special properties of NCs facilitate their biosensing applications,[41–46] such as the detection of bacteria.[47–49]

This review discusses current strategies using metal NCs (including gold, silver and copper (AuNCs, AgNCs, and CuNCs)) for the detection of bacteria. These sensor systems use a range of strategies to detect bacteria that are discussed in the course of this review (Figure 2). We also discuss future sensing trends using NCs, including their potential utility for theranostics.

2 Label-free detection of bacteria

2.1 Detection based on pH responsive behaviors

Bacteria can alter the pH value of the surrounding media.[50] For example growth of *E.coli* causes acidification of the surrounding media.[51] By means of this phenomenon, the concentration of *E. coli* was monitored using pH sensitive NCs. Xiong *et al* designed a pH monitoring system by the combination of dihydrolipoic acid protected AgNCs (DHLA-AgNCs) with agarose-LB (Luria-Bertani medium) hydrogels (Figure 3). The DHLA-AgNC-doped agarose hydrogels show brighter red emission with increasing pH value (Figure 3A, 3C). The red emission concomitantly decreases with increasing concentration of bacteria (Figure 3B). The weakest emission indicates the fully-grown colony of *E. coli* i.e the most acidic environment. Sensing by pH provides a rapid output, however, this approach is susceptible to environmental interference.

2.2 Agglomeration

Alteration of the optical behavior of NCs can occur through their interaction with bacterial cells. For instance, AuAgNCs are quenched by *A. baumannii* due to agglomeration (Figure 4).[53] This mechanism facilitates a facile route (ca. 40 minutes) to detect *A. baumannii* with a detection limit of 2.3×10^3 colony-forming unit (CFU)/mL. The intensity of the fluorescence decreased with increasing concentrations of *A. baumannii* from 1×10^4 to 5×10^7 CFU /mL and was almost completely quenched at 1×10^{10} CFU/mL (Figure 4B, C). The TEM (Figure 4D) for AuAgNCs after interaction with *A. baumannii* shows 30–200 nm size aggregates while no large size particles are observed for the *A. baumannii*-free micrograph.[54] Aggregation-induced quenching provides a promising transduction strategy for sensing of bacteria when integrated with effective and selective recognition processes.

2.3 Fluorescence recovery of metal ion-quenched NCs

Metal ions can bind with the components of bacterial cells; this binding can be used to provide a fluorescence displacement assay readout for bacteria. For instance, BSA-AuNCs

were quenched by Cu^{2+} and formed BSA-AuNC-Cu^{2+} adducts (Figure 5). Bacteria are known to reduce Cu^{2+} by various mechanisms. In the presence of *E. coli*, Cu^{2+} is reduced to Cu^{+} possibly by Ndh-2 (a cupric reductase), NADH dehydrogenase and other unknown pathways.[55–57] Cu^{+} can further diffuse through the cytoplasmic membrane. The reduction of Cu^{2+} and the removal of Cu^{+} results in the recovery of the fluorescence of BSA-AuNCs. Using this phenomenon, rapid detection of *E. coli* was achieved with a detection limit of 89 CFU/mL within 0.5 h. This on–off–on sensor can also screen multidrug-resistant bacteria in sepsis blood samples. However, the selectivity for specific bacteria is unknown. For instance, *Cupriavidus* sp. binds multiple metal ions including Cu^{2+}, resembling the activity of *E. coli*.[58]

3 Recognition through molecular motifs

3.1 Fluorescence sensing

3.1.1 Specific recognition strategies

3.1.1.1 Recognition of single receptors: NCs are smaller than many NPs[60] and can penetrate the cell membrane easily.[61, 62] Uptake of NCs by bacteria has been used for bacterial cell imaging, however, little selectivity is typically observed.[41] After decorating the NCs with elements that recognize receptors on bacterial cells, selectivity and uptake efficiency can be significantly improved. For instance, *E. coli* contains acyl homoserine lactone (AHL) receptors. Mukherji *et al* decorated AuNCs with AHL signal molecules that could recognize the Lux-R regulators within 2 h (Figure 6).[63] This functionalization allows differentiation of *E. coli* from *S. aureus* (10^6 cells/mL) suspensions that do not contain this receptor.

Further studies used highly fluorescent bovine serum albumin (BSA) protected AuNCs (quantum yield, 14%) functionalized with human anti-staphylococcal immunoglobulin (antiSAlgG) for specific imaging of *S.aureus* through fluorescence microscopy. The imaging of *S. aureus* can even be observed by naked eye under UV.[64] The studies were performed at physiological pH 7, showing an enhanced selectivity relative to nonspecific electrostatic binding of Au–human serum albumin NCs to *S. aureus*. In contrast to slow non-specific bacterial cell imaging by GSH-AuNCs (culture time, 24 hours), these specific AuNCs decorated with recognition element can be used for rapid imaging (< 2 h).[65]

3.1.1.2 Selective NC aggregation on bacterial cell wall: Enzymes such as lysozyme can recognize bacteria by binding to their membrane.[60, 66] For instance, the cell wall of *E. coli* contains a layer of peptidoglycan that is a specific site targeted by lysozyme. Lysozyme-protected AuNCs (Lysozyme-AuNCs) have recognition capabilities similar to lysozyme.[67–69] The Lysozyme-AuNCs (used as a fluorescent label) can attach to *E. coli*, providing turn-on fluorescence (Figure 7).[70] The fluorescence intensity of lysozyme-AuNCs changes linearly over the range of 2.4×10^4 – 6.0×10^6 CFU/mL with the limit of detection 2.0×10^4 CFU/mL for *E. coli*. The sensing time is about 5 minutes. This approach should be generalizable, and NCs protected with other cell wall recognition templates could also be employed to label and detect bacteria.

3.1.2 Dual recognition strategies

3.1.2.1 Magnetic enrichment: In magnetic enrichment methods, the analyte is attached to magnet beads (MB) and enriched by pulling down the beads using magnetic fields. Cheng *et al* developed a strategy for detection of *S. aureus* by combining two recognition molecules: a DNA aptamer and vancomycin (Van) (Figure 8).[71] The vancomycin-protected AuNCs (AuNCs@Van) bind onto the terminal residues (d-alanyl-d-alanine) of N-acetylmuramic acid and N-acetylglucosamine peptide subunits of *S. aureus*. The aptamer-MB specifically separates *S. aureus* by binding with the aptamer in the presence of magnetic field. The sandwiched structure is constructed by AuNCs@Van, *S. aureus* and aptamer-MB (after incubation at 37 °C for 3 h). Enhanced fluorescence is obtained by the enrichment of NCs in the sandwich structure, which increases as a function of the concentration of bacteria. The detection limit for *S. aureus* is 70 CFU/mL and the detection range is 99.8–103.3% with a standard deviation from 0.3 to 3.8%. This system using other bacteria species exhibits negligible enhancement in fluorescence intensity, demonstrating excellent selectivity.

In another study, nanocapsules with antibody-modified AuNCs embedded in chitosan (AuNCs@CS) and immunomagnetic nanoparticles were used to specifically recognize *E. coli* O157: H7 (Figure 9).[72] After separation by magnetic fields, *E. coli O157: H7* were isolated attached to the immunomagnetic nanoparticles and quantified by changes in fluorescence intensity of the AuNCs@CS linked to cells. Compared to traditional independent AuNC immunoassays, the AuNCs@CS nanocapsules amplified the fluorescence signal due to an increased number of fluorescent AuNCs binding to the *E. coli* O157:H7 cell (Figure 9b). The fluorescence intensity increases as a function of *E. coli* O157:H7 concentration. The magnetic separation captures 100% of *E. coli* O157:H7. The detection limit is 1 CFU/mL and the assay only requires 60 min. It is noteworthy that these dual-recognition strategies should all exhibit high sensitivity, selectivity and accuracy for detecting bacteria.

3.1.2.2 Fluorescence resonance energy transfer: Fluorescence resonance energy transfer (FRET) refers to an energy transfer process between fluorophore donors (accept photons and transfer energy) and acceptors. The optical properties of both donor and acceptor may change in the presence of analytes,[7374] which can be used to generate two or more signal channels or enhanced sensitivity. The FRET mechanism has been employed for detection of bacteria based on the application of NCs. For instance, *S. aureus* was detected by means of energy transfer from fluorescent AuNCs to non-fluorescent AuNPs (Figure 10).[75] In this sensing process, vancomycin-functionalized AuNCs act as a donor while the aptamer modified AuNPs serve as an acceptor. In the presence of *S. aureus*, the two moieties come in close proximity and the emission of the donor significantly changes due to FRET.[76] Using this strategy *S. aureus* (incubated at 37 °C for 30 min) was specifically quantified with a detection limit of 10 CFU/mL, demonstrating the potential benefits of FRET-based methods.

3.2 Catalysis

Catalysts can be used to accelerate reduction/oxidation reactions,[77] a strategy that has been applied to sensing. For instance, Huang *et al* developed a UV-assisted AuNC-chitosan composite sensor with an *S. aureus* specific aptamer.[78] *S. aureus* was attached to the

composite and catalyzed H_2O_2 decomposition to •OH radicals. 3,3,5,5-tetramethylbenzidine (TMB) was concomitantly oxidized to TMB (ox-TMB, blue color) by •OH radicals. The colorimetric readout of ox-TMB distinguishes *S. aureus* from other bacteria within 30 minutes. This method exhibits a detection limit of 1×10^2 CFU/mL. The catalytic activity of AuNCs is stable enough to resist 4 h of UV irradiation.

Another catalytic sensing strategy uses a nanoenzyme-triggered catalytic amplification strategy to detect *L. monocytogenes* based on AgNCs (Figure 11). The *o*-phenylenediamine (OPD) mediated aggregation of gold nanoparticles (GNPs) via NH-gold chemistry (Figure. 11a). In the absence of *L. monocytogenes*, no AgNCs can be captured by magnetic separation. GNPs, in contrast, were aggregated by the OPD (dark blue colour) indicator. *L. monocytogenes* could be captured by aptamer-modified magnetic beads and then recognized by immunoglobulin IgY-coated AgNCs (IgY-BSA-AgNCs) to form sandwich complexes. After magnetic separation, the AgNCs from the 'sandwich' catalyzed OPD conversion to oxidized OPD (ox-OPD). The colour of GNPs (red) were preserved because GNPs did not change with ox-OPD (Figure. 11b). The detection limit of this colorimetric sensor is 10 CFU/mL and the test time is ~30 minutes. providing excellent platform to monitor bacteria in complex system with little interference.

3.3 *In situ* synthesis of NCs

Bacterial components (e.g. proteins, polysaccharides, peptides) are potential templates for the growth of fluorescent NCs.[79, 80] This strategy has been used to sense and differentiate between bacterial strains. For example, bacterial cell walls can bind with the COOH group of 3-mercaptopropionic acid (MPA) and serve as a template for the synthesis of AuNCs. With changes in bacterial concentration, the fluorescence intensity changes with the generation of different amounts of AuNCs on the bacterial cell walls. In further experiment, kanamycin destroyed non-resistant bacterial cell walls while cell wall of resistant bacteria remained intact. Significant differences in the growth of AuNCs was observed for kanamycin-resistant strains in comparison to nonkanamycin-resistant strains after treating with kanamycin (Figure 12). Similarly, lysozyme damages the cell wall of Gram-positive bacteria but not Gram-negative bacteria, distinguishing Gram-positive from Gram-negative bacteria.[81]

Kaur's group combined the recognition capability of the antimicrobial peptide leucocin A (LeuA) and the *in situ* growth of 3-mercaptopropionic acid (MPA) protected AuNCs (MPA-AuNCs) for the detection of *L. monocytogenes*.[82] Leucocin A was immobilized on a glass surface to capture *L. monocytogenes* (Figure 13). The MPA-AuNCs (fluorescent label) were grown *in situ* on bacteria to generate fluorescence (Figure 13a). The detection limit was 2000 CFU using just 10 μL of sample with ca. 50 min assay time. This *in situ* generation of NCs provides a promising strategy for on-site bacterial detection.

3.4 Other fluorescence/catalysis methods

A number of molecular recognition motifs such as antibiotics, aptamers and peptides have been used to modify nanomaterials to enable selective/specific sensing (Table 1).[83].

4 Sensing arrays

The above-mentioned sensors were designed for detecting one type of bacteria using a recognition motif. An alternate strategy is to use array-based sensing strategies for detecting multiple types of bacteria.[90] For instance, human serum albumin (HSA), lysozyme (Lyz) and lactoferrin (Lf) protected NCs have been used for analysis of bacteria.[69, 89, 91] Li *et al* constructed a sensor array based on the combination of HSA-AuNCs, Lyz-AuNCs, Lf-AuNCs, and vancomycin functionalized HSA-AuNCs (Van-AuNCs) (Figure 14).[92] The first three probes identify the bacterial cells by the protein template. The last probe combines antibiotics with proteins to more specifically target the corresponding bacteria. Based on the sensing array, six types of bacterial cells including *A. faecalis*, *B. subtilis*, *S. aureus*, *E. coli*, MRSA (methicillin-resistant *S. aureus*) and KREC (kanamycin resistant *E. coli*) were discriminated. The bacteria could be identified at levels as low as as 1.2×10^7 cells/mL, with test time of 1 h. Wu *et al* reported a similar fluorescence sensing array based on metal ions modified AuNCs for analyzing bacterial cells.[93] The probes containing Zn^{2+}-Lys-AuNCs, Cd^{2+}-Lys-AuNCs, Zn^{2+}-BSA-AuNCs, Cd^{2+}-BSA-AuNCs, Zn^{2+}-HSAAuNCs, and Cd^{2+}-HSA-AuNCs were combined as the sensing array. The Gram-positive and −negative bacteria in suspensions (OD_{600} = 0.05) were differentiated and the test time was <30 minutes. Yang *et al.* fabricated a sensing array based on $^{(+)}$AuNPs/FA-AuAgNCs for the discrimination of sulfur-emitting bacteria.[94] The non-sulfur (*E. Coli*, *S.aures*) and sulfur-emitting bacteria (*C. thiooxidans*, *T. prufunda*, *A. Caldus SM-1*) were distinguished at ca. 30 minute at a level of OD_{600} = 0.005. These sensing arrays open up avenues for analyzing complicated bacterial infection systems.

5 Potential point-of-care applications

The fluorescence of NCs can change during antimicrobial processes, a phenomenon that could be employed for point-of care theranostics. In results that highlight this potential, Alsaiari *et al* designed a bacteria-responsive AuNCs@lysozyme-mesoporous silica (AuNCs@Lys-MSN) nanofiller for bacterial sensing and therapy (Figure 15). The electrostatic interaction between negatively-charged AuNCs@Lys and positively-charged aminated MSN provided an assembled drug carrier and detection system. In the presence of bacteria, AuNC@Lys detached from the MSN surface and the fluorescence of AuNC@Lys was quenched (Figure 15a). The release of entrapped kanamycin also occurred. The drug release system employed the adsorption of the AuNCs@Lys-MSN onto the bacteria upon bacterial contamination (Figure 15b), followed by the degradation of the bacterial cell wall by lysozyme that quenched the fluorescence of AuNCs. The fluorescence of AuNCs depended on the lysozyme catalytic activity and gradually quenched over time (Figure 15c).

In a different approach, an antibacterial polymer membrane containing AuNC@Lys-MSN loaded with kanamycin was fabricated on a photostimulable phosphor (PSP) plate as a theranostic device. The membrane shows bright red emission in absence of bacterial contamination. Upon encountering high bacterial contamination, the red emission was quenched as the detachment of AuNC@Lys from MSN while releasing the drugs (Figure 15d).

In yet another theranostic example, quaternary ammonium (QA) capped AuNCs were used for *in vivo* disinfection of MRSA. The live/dead bacteria can be differentiated at the same time using imaging method because the dissipated membrane charge of dead cells fails to bind QA-AuNCs.[96] The fabrication of more sensitive devices for theranostics of bacterial infection is still expected.[9798, 99] Most recently, NCs were used for *in-vivo* disease monitoring based on their catalysis effect and high renal clearance ability.[23] It indicates the *in-vivo* diagnosis of bacterial infection is very promising.

Conclusions

NCs provide a promising platform for detection and discrimination of bacteria. Unlike many metal NPs, NCs do not need covalent modification of fluorophores, which can reduce the complexity of the sensing strategy.NCs can detect bacteria without attachment of specific recognition elements, but the specificity is an area with substantial room for improvement. Appropriate engineering of NCs with recognition elements enable the NC-based probes with high specificity to recognize bacteria. NCs can grow *in situ* on bacterial cell walls and distinguish the targeted cells by treating with appropriate antibiotics. This *in situ* growth of NCs enable the on-site sensing of bacteria. Building on these single-element studies, NC-based sensing arrays have unique capabilities to identify different complex bacterial mixtures. Cs can also be used for theranostics and theranostics may be employed for future point-of-care diagnosis of bacterial infections. Despite the progress so far, efforts are required to improve the sensitivity, selectivity and practicality of NCs-based bacterial sensors. Additionally, integrating NC technology into devices will be required to enable point-of-care applications.

Supplementary Material

Refer to Web version on PubMed Central for supplementary material.

Acknowledgements

This work was supported by the NIH (AI AI134770). The authors also thank China Scholarship Council for the collaboration support to D.L.

Notes and references

1. Li B and Webster TJ, J Orthop Res, 2018, 36, 22–32. [PubMed: 28722231]
2. Smith PA, Koehler MFT, Girgis HS, Yan D, Chen Y, Chen Y, Crawford JJ, Durk MR, Higuchi RI, Kang J, Murray J, Paraselli P, Park S, Phung W, Quinn JG, Roberts TC, Rouge L, Schwarz JB, Skippington E, Wai J, Xu M, Yu Z, Zhang H, Tan MW and Heise CE, Nature, 2018, 561, 189–194. [PubMed: 30209367]
3. Silverman SM, Moses JE and Sharpless KB, Chemistry, 2017, 23, 79–83. [PubMed: 27747932]
4. McEwen SA, Angulo FJ, Collignon PJ and Conly JM, The Lancet Planetary Health, 2018, 2, e279–e282. [PubMed: 30074886]
5. Silver SBSKYLL, Biochemical pharmacology,, 2017, 133, 63–73. [PubMed: 28087253]
6. Stephan NCNCJVLKS, Drug Discovery Today, 2017, 22 234–248. [PubMed: 27890668]
7. Yong-Guan Zhu YZ, Li Bing, Huang Chu-Long, Zhang Si-Yu, Yu Shen, Chen Yong-Shan, Zhang Tong, Gillings Michael R., Su Jian-Qiang, Nature microbiology, 2017, 2, 16270

8. Saulnier D, De Decker S, Tourbiez D and Travers MA, J Microbiol Methods, 2017, 140, 67–69. [PubMed: 28709898]
9. Chakvetadze C, Purcarea A, Pitsch A, Chelly J and Diamantis S, IDCases, 2017, 8, 94–95. [PubMed: 28516038]
10. Ashraf A, Imran M, Yaqub T, Tayyab M, Shehzad W and Thomson PC, Mol Cell Probes, 2017, 33, 57–64. [PubMed: 28336361]
11. Marx V, Nature Methods, 2017, 14, 37–40.
12. Durand ML, Clin Microbiol Rev, 2017, 30, 597–613. [PubMed: 28356323]
13. Sui Ching Phung JMC, Macka Mirek, Shane, Powell M, Guijt Rosanne M, and Breadmore Michael C., Analytical Chemistry, 2017, 89 6513–6520. [PubMed: 28528550]
14. Leng X, Wang Y, Liu S, Pei Q, Cui X, Tu Y, Liu X and Huang J, Sensors and Actuators B: Chemical, 2017, 252, 689–696.
15. Bhardwaj N, Bhardwaj SK, Nayak MK, Mehta J, Kim K-H and Deep A, TrAC Trends in Analytical Chemistry, 2017, 97, 120–135.
16. Xue L, Zheng L, Zhang H, Jin X and Lin J, Sensors and Actuators B: Chemical, 2018, 265, 318–325.
17. Yang B, Chen B, He M and Hu B, Anal Chem, 2017, 89, 1879–1886. [PubMed: 28208247]
18. Hu RR, Yin ZZ, Zeng YB, Zhang J, Liu HQ, Shao Y, Ren SB and Li L, Biosens Bioelectron, 2016, 78, 31–36. [PubMed: 26584080]
19. Chen J, Andler SM, Goddard JM, Nugen SR and Rotello VM, Chem Soc Rev, 2017, 46, 1272–1283. [PubMed: 27942636]
20. Cifuentes-Rius A, Ivask A, Das S, Penya-Auladell N, Fabregas L, Fletcher NL, Houston ZH, Thurecht KJ and Voelcker NH, ACS Appl Mater Interfaces, 2017, 9, 41159–41167. [PubMed: 29116739]
21. Sultan D, Ye D, Heo GS, Zhang X, Luehmann H, Yue Y, Detering L, Komarov S, Taylor S, Tai YC, Rubin JB, Chen H and Liu Y, Small, 2018, 14, e1703115. [PubMed: 29966035]
22. Nair LV, Nair RV, Shenoy SJ, Thekkuveettil A and Jayasree RS, Journal of Materials Chemistry B, 2017, 5, 8314–8321. [PubMed: 32264500]
23. Loynachan CN, Soleimany AP, Dudani JS, Lin Y, Najer A, Bekdemir A, Chen Q, Bhatia SN and Stevens MM, Nat Nanotechnol, 2019, DOI: 10.1038/s41565-019-0527-6, in press.
24. Zhang J, Li Z, Huang J, Liu C, Hong F, Zheng K and Li G, Nanoscale, 2017, 9, 16879–16886. [PubMed: 29075729]
25. Chakraborty I and Pradeep T, Chem Rev, 2017, 117, 8208–8271. [PubMed: 28586213]
26. Li H, Li L, Pedersen A, Gao Y, Khetrapal N, Jonsson H and Zeng XC, Nano Lett, 2015, 15, 682–688. [PubMed: 25493586]
27. Higaki T, Zhou M, Lambright KJ, Kirschbaum K, Sfeir MY and Jin R, J Am Chem Soc, 2018, 140, 5691–5695. [PubMed: 29658712]
28. Li D, Chen Z, Wan Z, Yang T, Wang H and Mei X, RSC Advances, 2016, 6, 34090–34095.
29. Dipankar Bain SM, Paramanik Bipattaran, Patra Amitava, ACS Sustainable Chem. Eng, 2018, 6, 2334–2343.
30. Wu Z and Jin R, Nano Lett, 2010, 10, 2568–2573. [PubMed: 20550101]
31. Chen Y, Yang T, Pan H, Yuan Y, Chen L, Liu M, Zhang K, Zhang S, Wu P and Xu J, J Am Chem Soc, 2014, 136, 1686–1689. [PubMed: 24437963]
32. Muhammad U. Farooq VN, Rozhkova Elena A., Sci Rep, 2018, 8, 2907. [PubMed: 29440698]
33. Yin M-M, Chen W-Q, Liu Y and Jiang F-L, ACS Applied Nano Materials, 2019, 2, 408–417.
34. Liu Y, Wang J, Song X, Xu K, Chen H, Zhao C and Li J, Microchim Acta, 2018, 185, 360.
35. Li D, Chen Z and Mei X, Adv Colloid Interface Sci, 2017, 250, 25–39. [PubMed: 29132640]
36. Cui Y, Yang J, Zhou Q, Liang P, Wang Y, Gao X and Wang Y, ACS Appl Mater Interfaces, 2017, 9, 5900–5906. [PubMed: 28111943]
37. Zheng Y, Lai L, Liu W, Jiang H and Wang X, Adv Colloid Interface Sci, 2017, 242, 1–16. [PubMed: 28223074]

38. Jiao Zhai LZ, Zheng Lingna, Gao Fuping, Gao Liang, Liu Ru, Wang Yaling, Gao Xueyun, ACS Omega, 2017, 2, 276–282. [PubMed: 30023515]
39. Rong Yan ZS, Chen Jie, Wu Hao, Zhao Yuan, Qiu Lin, Jiang Pengju, Mou Xiao Zhou, Wang Jian Hao, and Li Yong Qiang, ACS Sustainable Chem. Eng, 2018, 6, 4504–4509.
40. Song Y, Gutiérrez OY, Herranz J and Lercher JA, Applied Catalysis B: Environmental, 2016, 182, 236–246.
41. Chen LY, Wang CW, Yuan Z and Chang HT, Anal Chem, 2015, 87, 216–229. [PubMed: 25275676]
42. Zhang L and Wang E, Nano Today, 2014, 9, 132–157.
43. Jin R, Zeng C, Zhou M and Chen Y, Chem Rev, 2016, 116, 10346–10413. [PubMed: 27585252]
44. Mao B, Qu F, Zhu S and You J, Sensors and Actuators B: Chemical, 2016, 234, 338–344.
45. Xiaoning Li SMR, Gupta Akash, Saha Krishnendu, Jiang Ziwen, Moyano Daniel F., Sahar Ali, Riley Margaret A., and Rotello Vincent M., ACS Nano, 2014, 8, 10682–10686. [PubMed: 25232643]
46. Jiang X, Du B, Huang Y and Zheng J, Nano Today, 2018, 21, 106–125. [PubMed: 31327979]
47. Siamak Javani RL, Latorre Alfonso, Flors Cristina, Cortajarena Aitziber L., and Somoza Álvaro, ACS Appl. Mater. Interfaces, 2016, 8, 10147–10154. [PubMed: 27058628]
48. Wang HY, Hua XW, Wu FG, Li B, Liu P, Gu N, Wang Z and Chen Z, ACS Appl Mater Interfaces, 2015, 7, 7082–7092. [PubMed: 25785786]
49. Mishra SK, Raveendran S, Ferreira JM and Kannan S, Langmuir, 2016, 32, 10305–10316. [PubMed: 27685160]
50. Park JH, Kumar G, Park JH, Park HD and Kim SH, Bioresour Technol, 2015, 188, 109–116. [PubMed: 25683506]
51. Ara Koh FDV, Kovatcheva-Datchary Petia, Backhed Fredrik, Cell, 2016, 6, 1332–1345.
52. Xiong H, Zheng H, Wang W, Liang J, Wen W, Zhang X and Wang S, Biosens Bioelectron, 2016, 86, 164–168. [PubMed: 27371824]
53. Zheng Y, Wang X and Jiang H, Sensors and Actuators B: Chemical, 2018, 277, 388–393.
54. Yang Y, Han A, Li R, Fang G, Liu J and Wang S, Analyst, 2017, 142, 4486–4493. [PubMed: 29094138]
55. Durgadas CV, Sharma CP and Sreenivasan K, Analyst, 2011, 136, 933–940. [PubMed: 21152627]
56. Rensing C and Grass G, FEMS Microbiology Reviews, 2003, 27, 197–213. [PubMed: 12829268]
57. Solioz M, Mycobacterial Diseases, 2016, 6, 1000210.
58. Yang Y, Hu M, Zhou D, Fan W, Wang X and Huo M, RSC Advances, 2017, 7, 18793–18802.
59. Rong Yan ZS, Chen Jie, Wu Hao, Zhao Yuan, Qiu Lin, Jiang Pengju, Mou Xiao-Zhou, Wang Jianhao, Li Yong-Qiang, ACS Sustainable Chem. Eng, 2018, 6, 4504–4509.
60. Baker M, Nature Methods, 2010, 7, 957–962.
61. Liu Z, Jing X, Zhang S and Tian Y, Anal Chem, 2019, 91, 2488–2497. [PubMed: 30618245]
62. Pranantyo D, Liu P, Zhong W, Kang ET and Chan-Park MB, Biomacromolecules, 2019, DOI: 10.1021/acs.biomac.9b00392, 2922–2933. [PubMed: 31305998]
63. Mukherji R, Samanta A, Illathvalappil R, Chowdhury S, Prabhune A and Devi RN, ACS Appl Mater Interfaces, 2013, 5, 13076–13081. [PubMed: 24266726]
64. Khlebtsov B, Tuchina E, Tuchin V and Khlebtsov N, RSC Advances, 2015, 5, 61639–61649.
65. Kong L, Chu X, Ling X, Ma G, Yao Y, Meng Y and Liu W, Microchimica Acta, 2016, 183, 2185–2195.
66. Linda Eriksson PLH, Ingegerd Johansson, Scientific Reports, 2017, 7, 5861. [PubMed: 28724921]
67. Russell BA, Jachimska B, Komorek P, Mulheran PA and Chen Y, Phys Chem Chem Phys, 2017, 19, 7228–7235. [PubMed: 28234394]
68. Wang X, Cao W, Xiang Q, Jin F, Peng X, Li Q, Jiang M, Hu B and Xing X, Mater Sci Eng C Mater Biol Appl, 2017, 76, 886–896. [PubMed: 28482604]
69. Liu J, Lu L, Xu S and Wang L, Talanta, 2015, 134, 54–59. [PubMed: 25618640]
70. Goswami N, Yao Q, Luo Z, Li J, Chen T and Xie J, J Phys Chem Lett, 2016, 7, 962–975. [PubMed: 26912457]

71. Cheng D, Yu M, Fu F, Han W, Li G, Xie J, Song Y, Swihart MT and Song E, Anal Chem, 2016, 88, 820–825. [PubMed: 26641108]
72. Cheng C, Yang L, Zhong M, Deng W, Tan Y, Xie Q and Yao S, Analyst, 2018, 143, 4067–4073. [PubMed: 30062360]
73. Li D, Wang G, Peng Y, Chen Z, Gao X, Cheng L and Mei X, Nanoscale Advances, 2019, 1, 1086–1095.
74. Wang Q, Wang X, Sun Y, Yang X, Zhang L, Zhang Q, Hu ZQ and Hu HY, Chem Commun (Camb), 2019, 55, 5064–5067. [PubMed: 30896004]
75. Yu M, Wang H, Fu F, Li L, Li J, Li G, Song Y, Swihart MT and Song E, Anal Chem, 2017, 89, 4085–4090. [PubMed: 28287715]
76. Krainer G, Hartmann A and Schlierf M, Nano Lett, 2015, 15, 5826–5829. [PubMed: 26104104]
77. Creran B, Li X, Duncan B, Kim CS, Moyano DF and Rotello VM, ACS Appl Mater Interfaces, 2014, 6, 19525–19530. [PubMed: 25318086]
78. Xie X, Tan F, Xu A, Deng K, Zeng Y and Huang H, Sensors and Actuators B: Chemical, 2019, 279, 289–297.
79. Ding H, Li H, Liu P, Hiltunen JK, Wu Y, Chen Z and Shen J, Microchimica Acta, 2014, 181, 1029–1034.
80. Goswami U, Sahoo AK, Chattopadhyay A and Ghosh SS, ACS Omega, 2018, 3, 6113–6119. https://pubs.acs.org/doi/10.1021/acsomega.8b00504. [PubMed: 30023939]
81. West AL, Schaeublin NM, Griep MH, Maurer-Gardner EI, Cole DP, Fakner AM, Hussain SM and Karna SP, ACS Appl Mater Interfaces, 2016, 8, 21221–21227. [PubMed: 27328035]
82. Hossein-Nejad-Ariani H, Kim T and Kaur K, ACS Applied Nano Materials, 2018, 1, 3389–3397.
83. Wang LS, Gopalakrishnan S and Rotello VM, Langmuir, 2018, DOI: 10.1021/acs.langmuir.8b03235, in press.
84. Leng X, Wang Y, Li R, Liu S, Yao J, Pei Q, Cui X, Tu Y, Tang D and Huang J, Microchim Acta, 2018, 185, 168.
85. Zheng L, Qi P and Zhang D, Sensors and Actuators B: Chemical, 2018, 276, 42–47.
86. Ye Y, Liu Y, He S, Xu X, Cao X, Ye Y and Zheng H, Sensors and Actuators B: Chemical, 2018, 272, 53–59.
87. Lin X, Liu Y, Deng J, Lyu Y, Qian P, Li Y and Wang S, Chemical Science, 2018, 9, 1774–1781. [PubMed: 29675221]
88. Chan PH, Ghosh B, Lai HZ, Peng HL, Mong KK and Chen YC, PLoS One, 2013, 8, e58064. [PubMed: 23554874]
89. Chan PH and Chen YC, Anal Chem, 2012, 84, 8952–8956. [PubMed: 23088348]
90. Geng Y, Peveler WJ and Rotello V, Angew Chem Int Ed Engl, 2019, 58, 5190–5200. [PubMed: 30347522]
91. Xavier PL, Chaudhari K, Verma PK, Pal SK and Pradeep T, Nanoscale, 2010, 2, 2769–2776. [PubMed: 20882247]
92. Ji H, Wu L, Pu F, Ren J and Qu X, Adv Healthc Mater, 2018, 7, 1701370.
93. Wu Y, Wang B, Wang K and Yan P, Analytical Methods, 2018, 10, 3939–3944.
94. Yang JY, Yang T, Wang XY, Wang YT, Liu MX, Chen ML, Yu YL and Wang JH, Anal Chem, 2019, 91, 6012–6018. [PubMed: 30964645]
95. Alsaiari SK, Hammami MA, Croissant JG, Omar HW, Neelakanda P, Yapici T, Peinemann KV and Khashab NM, Adv Healthc Mater, 2017, 6, 1601135.
96. Xie Y, Liu Y, Yang J, Liu Y, Hu F, Zhu K and Jiang X, Angew Chem Int Ed Engl, 2018, 57, 3958–3962. [PubMed: 29423995]
97. Li LL and Wang H, Adv Healthc Mater, 2013, 2, 1351–1360. [PubMed: 23526816]
98. Zhou W, Le J, Chen Y, Cai Y, Hong Z and Chai Y, TrAC Trends in Analytical Chemistry, 2019, 112, 175–195.
99. Tsuru A, Setoguchi T, Kawabata N, Hirotsu M, Yamamoto T, Nagano S, Yokouchi M, Kakoi H, Kawamura H, Ishidou Y, Tanimoto A and Komiya S, BMC Res Notes, 2015, 8, 288. [PubMed: 26138214]

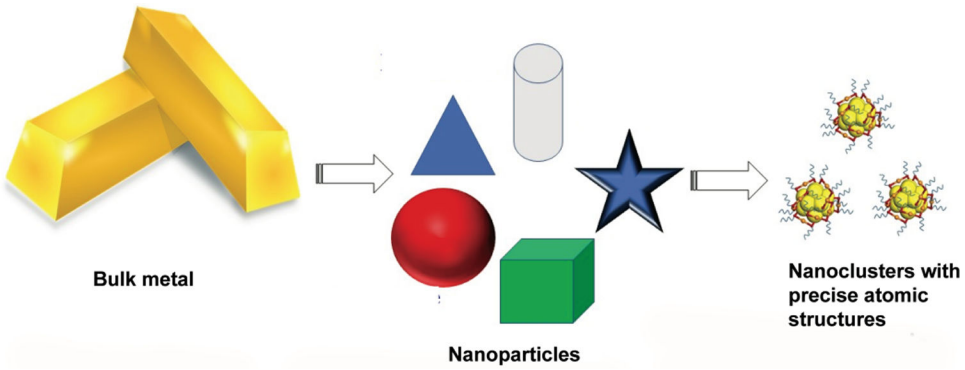

Figure 1.
From bulk metal to atomic-precise NCs.

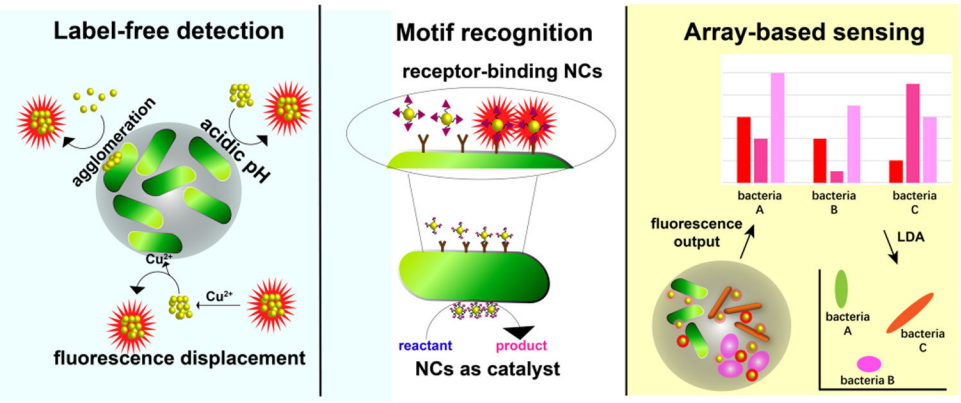

Figure 2.
Overview of NCs-based bacterial sensing strategies.

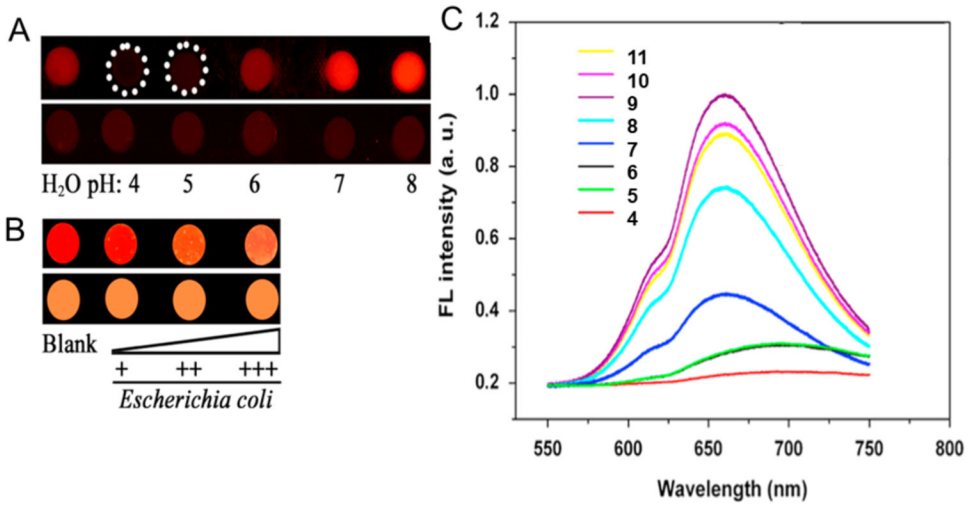

Figure 3.

(A) Fluorescence probes for pH using DHLA-AgNCs-doped agarose hydrogels (upper) and agarose hydrogels (lower) under UV-light irradiation. (B) Monitoring of bacterial growth using DHLA-AgNCs-doped agarose-LB hydrogels (upper) and LB solid medium (lower) under UV light irradiation. (C) Fluorescence emission spectra of AgNCs at different pH values (excitation at 432 nm). Adapted with permission from ref.[52] Copyright 2016 Elsevier Ltd.

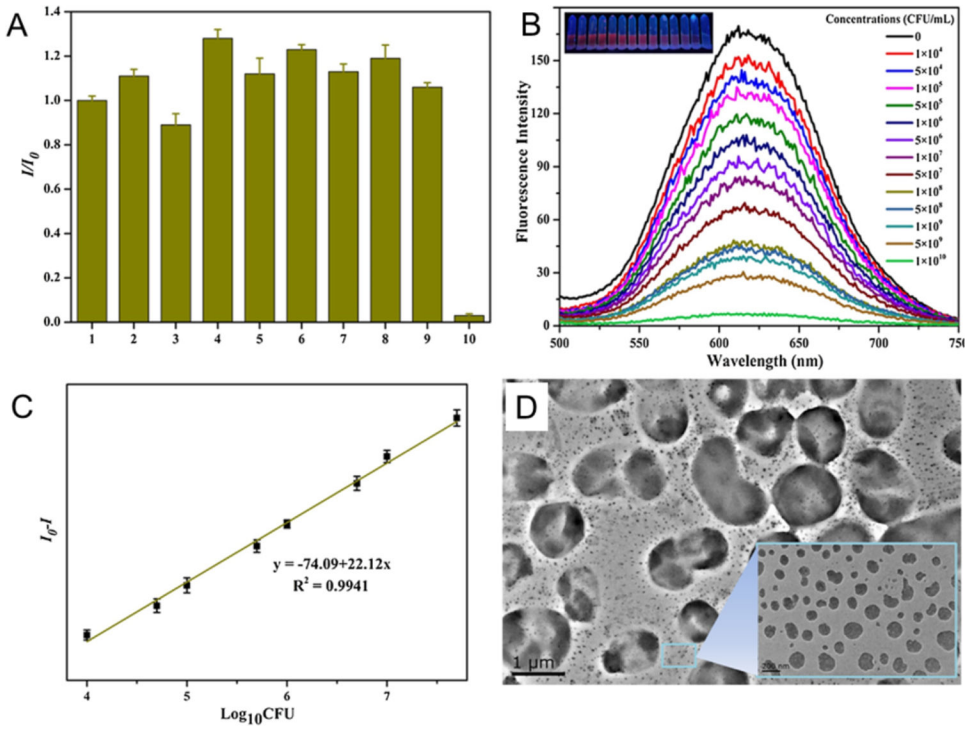

Figure 4.

Highly fluorescent AuAgNCs recognizes *A. baumannii* with high selectivity and sensitivity. (A) The fluorescence of AuAgNCs was quenched by *A. baumannii* but not by other strains. The numbers 1–10 represent control, *B. mycoides*, *S. aureus*, MRSA, *C. albicans*, *P. aeruginosa*, *E. coli*, VRE, *S. cerevisiae*, and *A. baumannii*, respectively. (B) The quenching of AuAgNCs in different concentration of *A. baumannii*. Insets: Photos of *A. baumannii* treated with AuAgNCs under UV light. (C) Relative fluorescence intensity (I_0-I) of AuAgNCs as a function of the logarithm of the *A. baumannii* concentration. (D) The TEM image of AuAgNCs treated with 1×10^5 CFU/mL of *A. baumannii*. Adapted with permission from ref.[53] Copyright 2016 Elsevier Ltd.

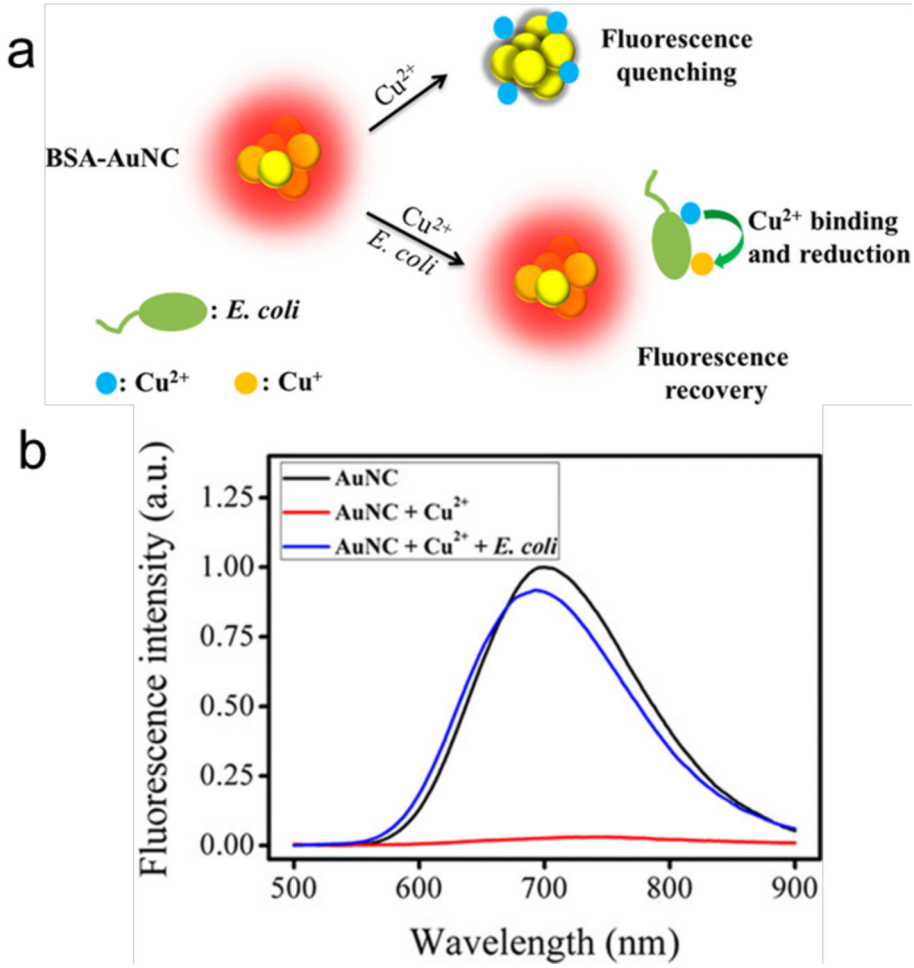

Figure 5.

(a) Schematic illustration of the on-off-on AuNCs-based fluorescent probe for rapid *E. coli* detection. (b) Fluorescence emission spectra of AuNCs (1 μM) and AuNCs-Cu^{2+} ensemble (1 μM of AuNCs, 4 μM of Cu^{2+}) with and without *E. coli* (10^6 CFU/mL) incubation. Reproduced from Ref.[59] Copyright 2018 American Chemical Society.

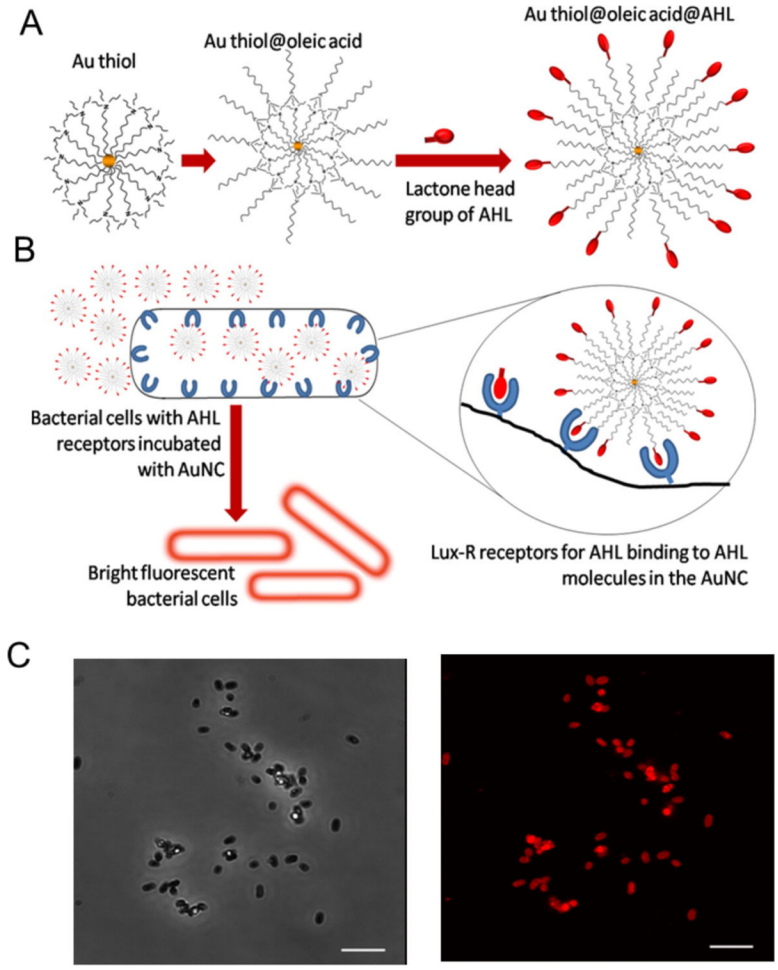

Figure 6.

Fabrication of fluorescent probes for bacterial cells: (A) Structure of the probe with AHL signal molecules deployed on the surface with lactone and amide moieties intact and (B) Specific binding of AHL head groups to receptor sites in Lux-R regulators with bacteria. (C) Confocal microscopy images of *E. coli* incubated with Au@OA@C8-AHL (AuNC probe functionalized with AHL signal molecules): (top) phase contrast image and (bottom) fluorescence image of the same region. Scale bar is 5 μm. Reproduced from ref.[63] with permission from The Royal Society of Chemistry.

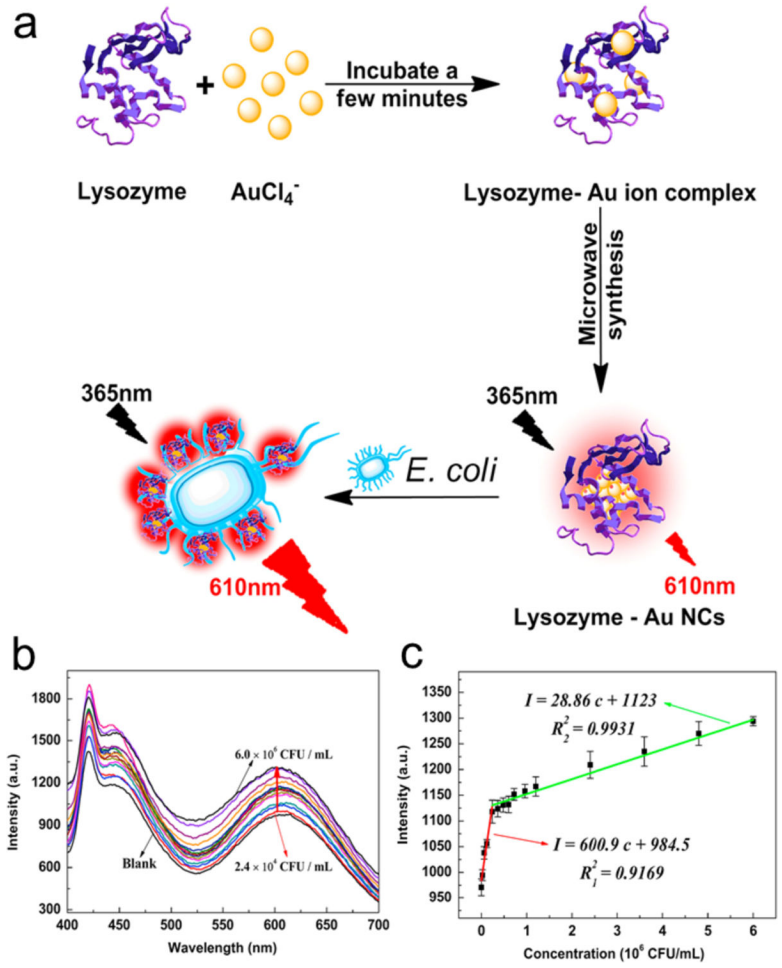

Figure 7.

(a) Synthesis of the red-emitting lysozyme-AuNCs and fluorescence enhancement for the analysis of *E. coli*. (b) Evolution of fluorescence spectra of lysozyme-AuNCs with varying *E. coli* concentrations. (c) The calibration plots of red fluorescence intensity vs *E. coli* concentrations, $\lambda_{ex}/\lambda_{em}$=365 nm/610 nm. Adapted with permission from ref.[69] Copyright 2015 Elsevier Ltd.

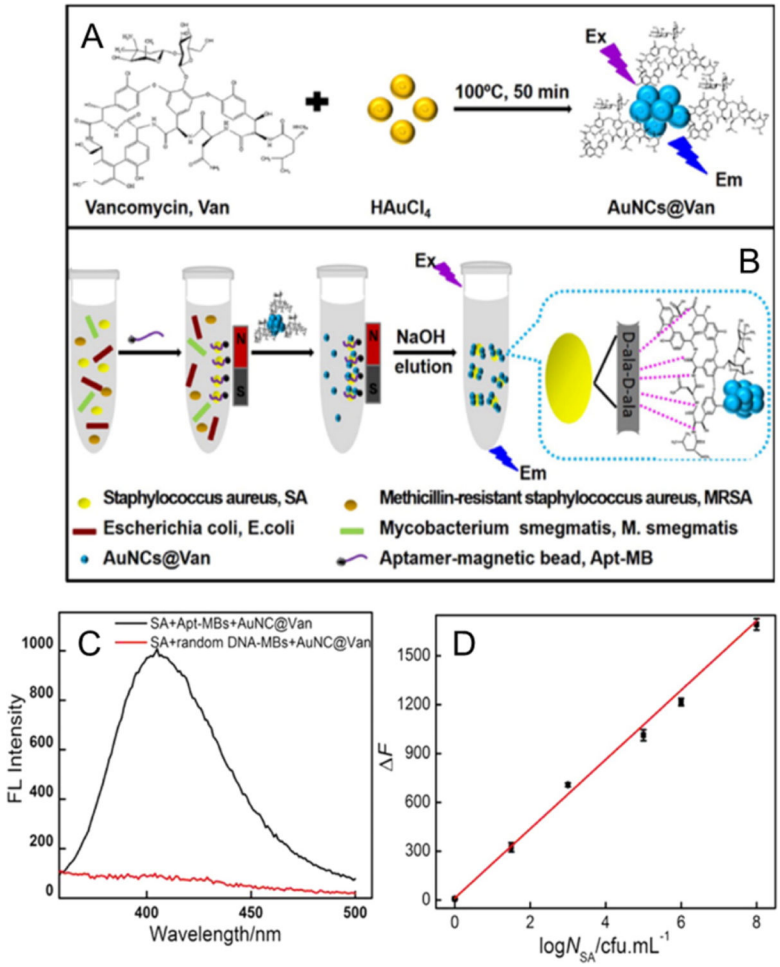

Figure 8.

(A) Schematic illustrations of the preparation of AuNCs@Van, (B) and determination of *S.aureus* in mixtures using the aptamer-MB and AuNCs@Van dual recognition strategy. (C) Fluorescence spectra of detected *S. aureus* with aptamer-MBs or random DNA-MBs and AuNCs@Van. (D) The linear regression curve of the enhanced fluorescence intensity (ΔF, at 412 nm) vs. the concentration of *S. aureus* (log NSA/CFU mL^{-1}). Reproduced from Ref.[71] Copyright 2016 American Chemical Society.

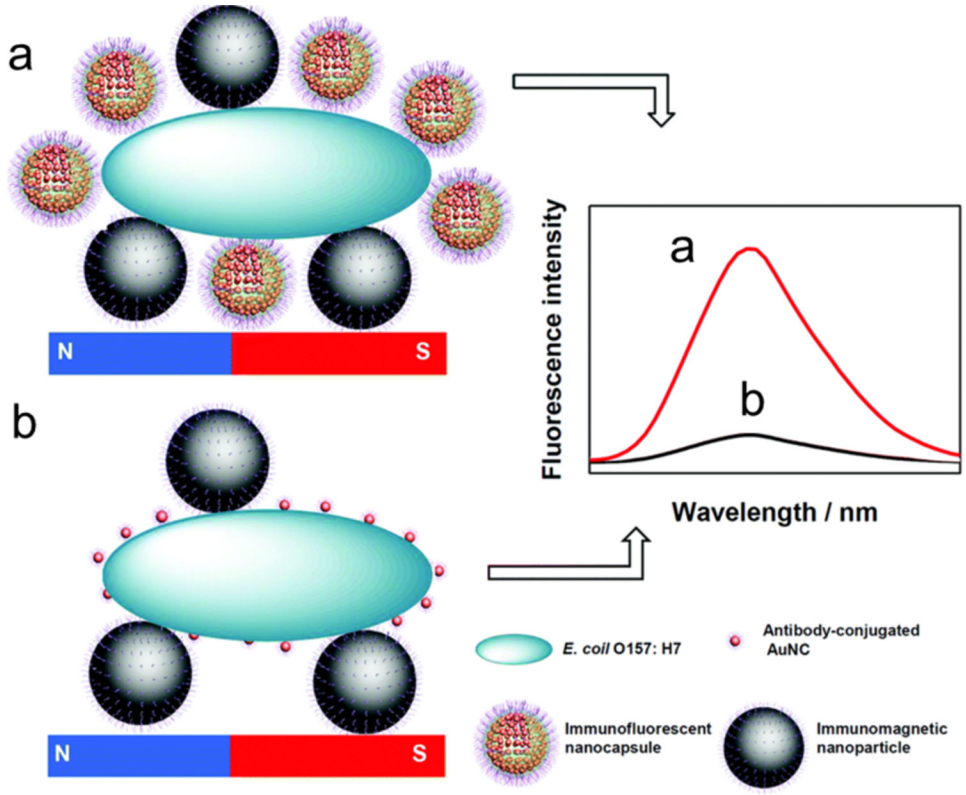

Figure 9.

Illustration of the immunoassay of *E. coli O157:H7* using (a) AuNCs@CS nanocapsules and (b) independent AuNCs as labels. Reproduced with permission from ref.[72] Copyright 2018 The Royal Society of Chemistry.

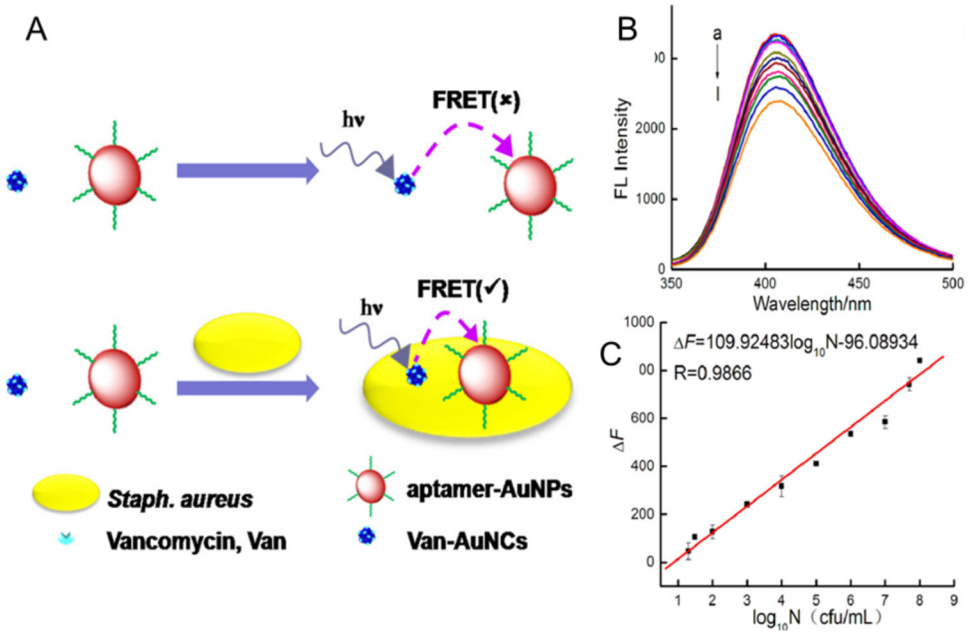

Figure 10.

(A) Illustration of the vancomycin and aptamer dual-recognition FRET assay for detection of *S. aureus)* (B) Fluorescence spectra of the FRET biosensor in the presence of *S. aureus* at varying concentrations (curves a-l correspond to 0, 10, 20, 30, 10^2, 10^3, 10^4, 10^5, 10^6, 10^7, 5 × 10^7 and 10^8 CFU/mL, respectively). (C) Calibration curve showing the linear relationship between fluorescence intensity and the logarithm of *S. aureus* concentration ($\log_{10}N$ CFU/mL). Reproduced with permission from ref.[75] Copyright 2018 American Chemical Society

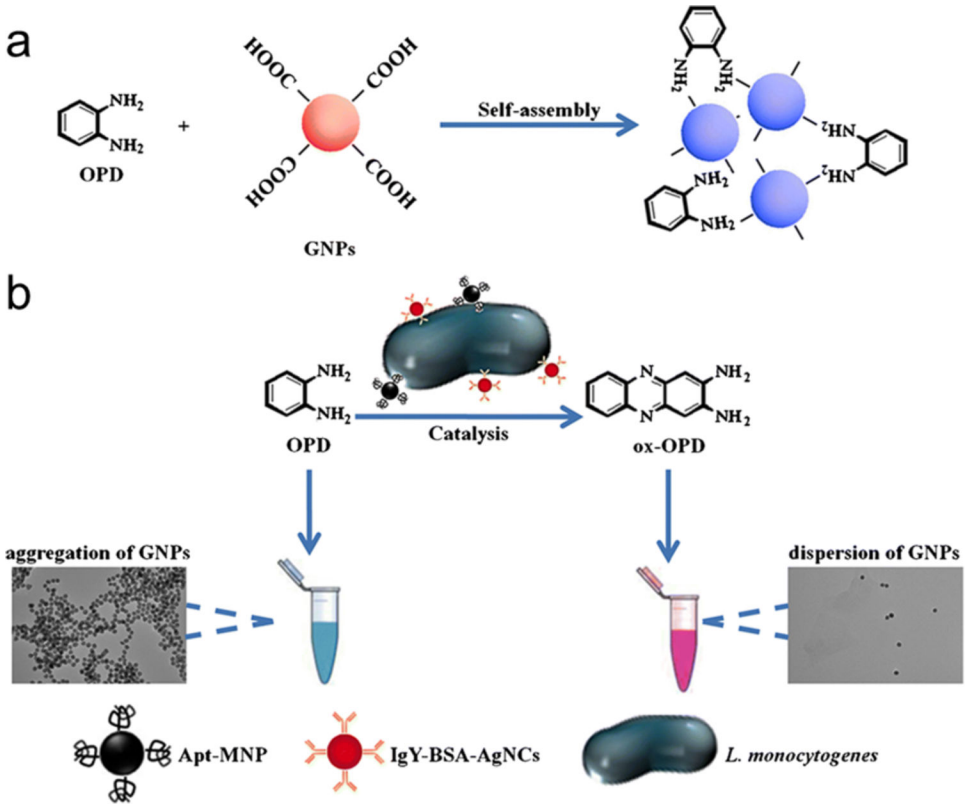

Figure 11.

Schematic representation of the colorimetric detection of *L. monocytogenes*. (a) OPD causes the aggregation of AuNPs. (b) The IgY-BSA-AgNCs attached onto the sandwich-type immunocomplex for catalytic oxidization of OPD to produce ox-OPD. Adapted with permission from ref.[34] Copyright 2018 Springer Nature.

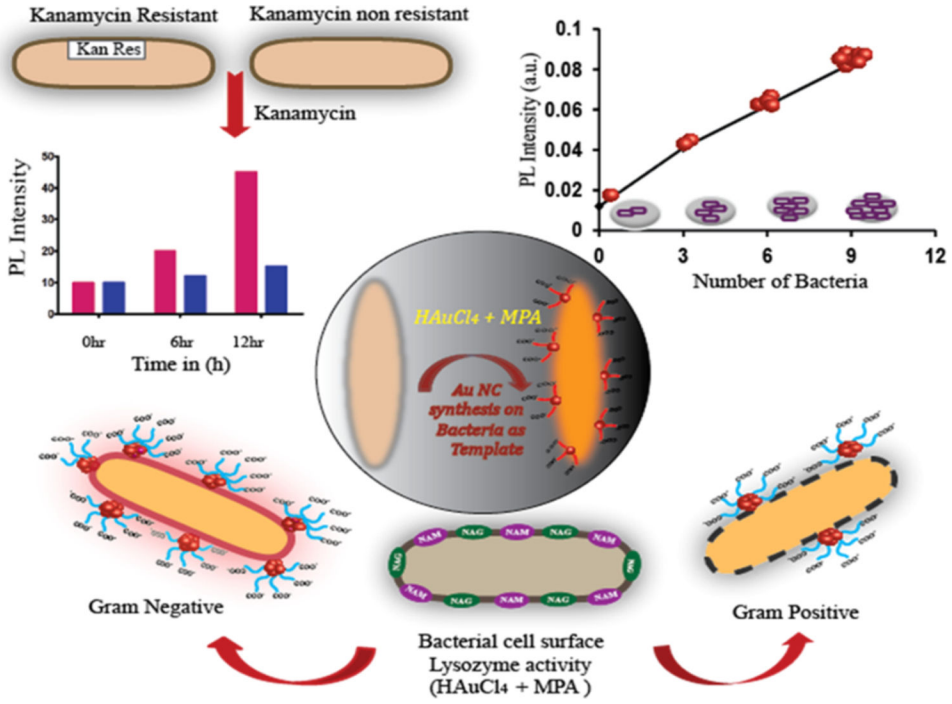

Figure 12.

Schematic representation of AuNCs synthesized on bacterial cell wall and the differentiation between Gram-Positive and Gram-Negative Bacteria. Reproduced from Ref.[80] Copyright 2018 American Chemical Society. Further permissions related to the material excerpted should be directed to the ACS.

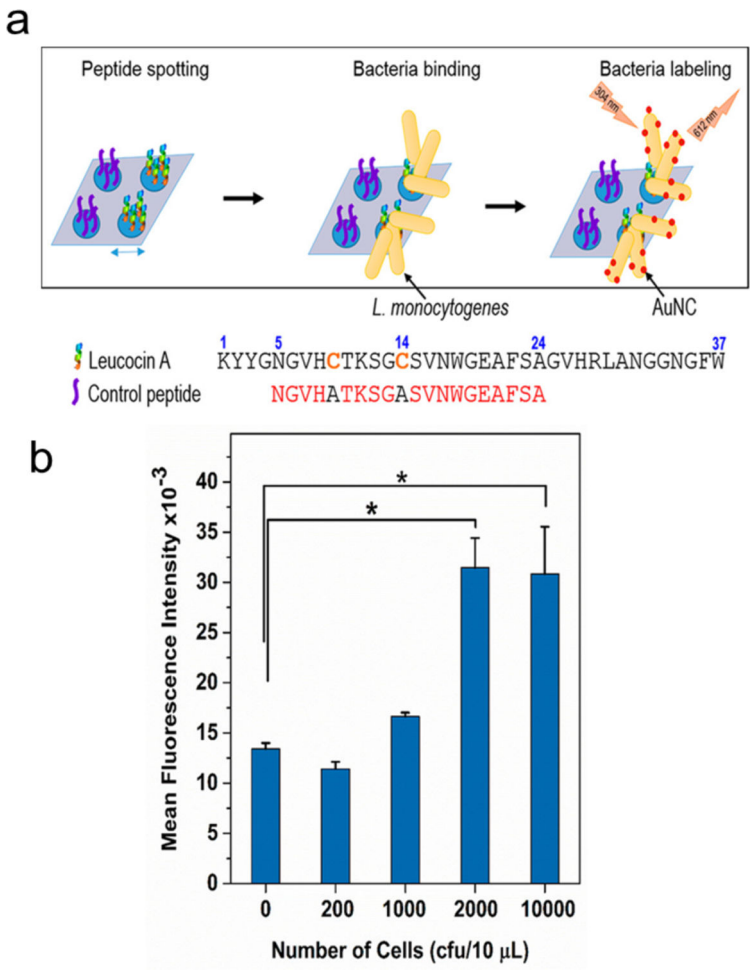

Figure 13.

(a) Scheme for the specific detection of *Listeria monocytogenes* using leucocin A (LeuA) and AuNCs. (b) Fluorescence response of bound bacteria with increasing bacterial concentration (*L. monocytogenes*) per spot. Peptide LeuA (10 μL, 0.1 mM) was spotted on glass slide followed by bacteria (10 μL) and MPA-AuNCs (12 μL). Reproduced from Ref.[82] Copyright 2018 American Chemical Society.

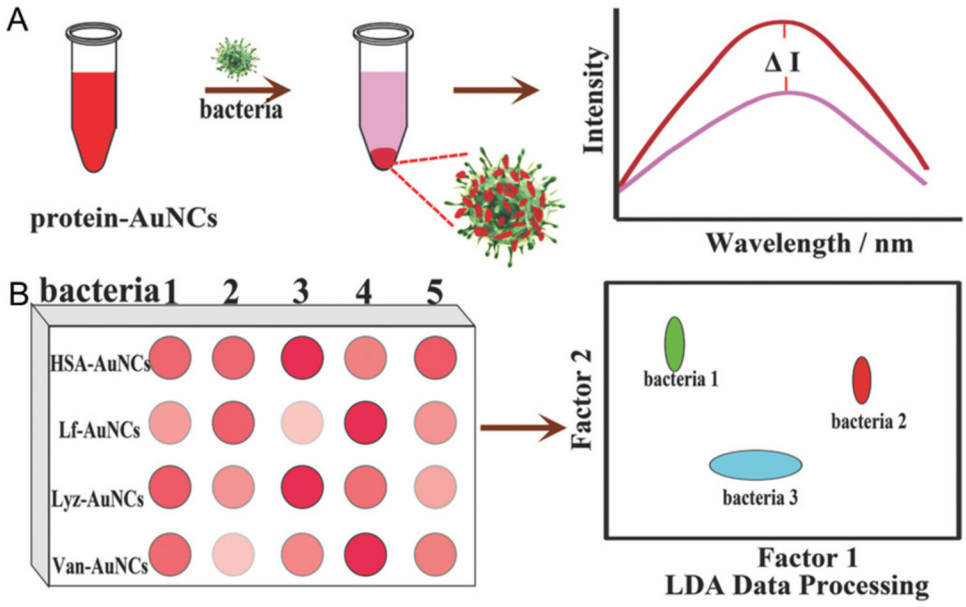

Figure 14.

Schematic illustration of protein protected AuNCs-based fluorescence sensing array for discrimination of bacteria. A) The fluorescence intensities of the protein-AuNCs were significantly reduced in the presence of bacteria. B) Fluorescence pattern generated from the different responses of the protein-AuNCs probes toward bacteria. Reproduced with permission from ref.[92] Copyright 2018 The Royal Society of Chemistry.

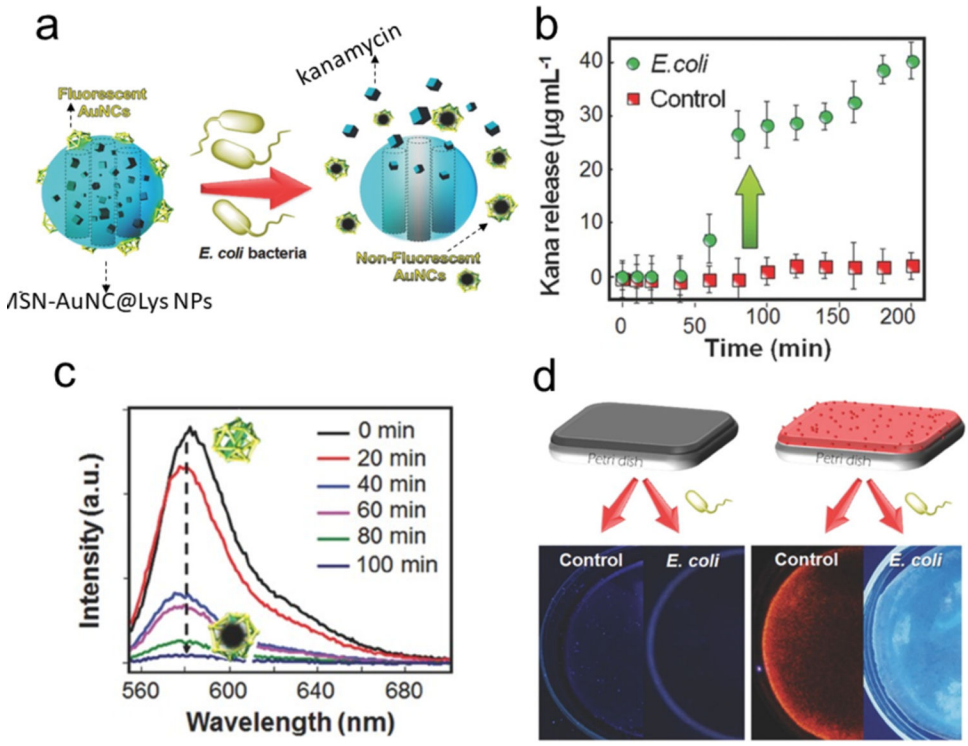

Figure 15.

a) Illustration of the bacteria-triggered cargo release from MSNAuNC@Lys NPs and the simultaneous quenching of fluorescence upon the E. coli exposure (kanamycin represented by cubes). b) Kanamycin release profiles from the mixed membrane in the presence of *E. coli* bacteria or in LB broth. c) Fluorescence emission spectra of AuNC@Lys: as the activity of lysozyme increases, the fluorescence of AuNCs decreases. d) The nanofiller-free and nanofiller-doped membranes was immersed with and without *E. coli* containing broth. Adapted with permission from ref.[95] Copyright 2017 Wiley-VCH Verlag GmbH & Co. KGaA, Weinheim.

Table 1

Sensors based on the optical or catalytic properties of NCs for recognition of bacteria through the identification by a molecular motif.

NCs	Molecular motif	Bacteria	The Advantage from NCs	Detection Limit	Ref.
DNA-AgNCs	Aptamer	*S. typhimurium*,	Fluorescence	8 CFU/mL	84
DNA-AgNCs	DNAzyme	*E. coli*	Fluorescence	60 CFU/mL	85
DNA-AgNCs	Aptamer	*Salmonella*	Catalysis	0.97 fM	86
DNA-AgNCs	Aptamer	*E. coli, S. aureus*	Fluorescence	100 fM	87
CHI-AuNCs	Aptamer	*S. aureus*, SE-B	Catalysis	1.0×10^{-12} g/mL	78
BSA-AuNCs	AntiSAIgG	MSSA and MRSA	Fluorescence	-	64
AuNCs@Mann	Mannose	*E. coli J96*	Fluorescence	2×10^6 cells/mL	88
HSA-AuNCs	Peptide	*S. aureus, MRSA*	Fluorescence	106 cells/mL	89
Pep-AuNCs	Peptide	*Listeria monocytogenes*	Fluorescence	2000 CFU/mL	82

*CHI- chitosan; HSA - human serum albumin; Pep- peptide; Mann-mannose; MSSA- methicillin-susceptible Staphylococcus aureus; MRSA-methicillin-resistant Staphylococcus aureus; SE-B-Staphylococcal enterotoxin B.